POLITECNICO DI TORINO
Repository ISTITUZIONALE

Hybrid Fidelity Optimization of Efficient Airfoils and Rotors in Ultra-Low Reynolds Numbers Conditions

(Article begins on next page)

16 May 2024

Hybrid Fidelity Optimization of Efficient Airfoils and Rotors in Ultra-Low Reynolds Numbers Conditions

2 authors:

Manuel Carreño Ruiz
Politecnico di Torino
13 PUBLICATIONS **39** CITATIONS

SEE PROFILE

Domenic D'Ambrosio
Politecnico di Torino
57 PUBLICATIONS **557** CITATIONS

SEE PROFILE

Some of the authors of this publication are also working on these related projects:

Electromagnetic fluid dynamics for aerospace applications View project

Hybrid Fidelity Optimization of Efficient Airfoils and Rotors in Ultra-Low Reynolds Numbers Conditions

M. Carreño Ruiz [*] and D. D'Ambrosio [†]

Department of Mechanical and Aerospace Engineering, Politecnico di Torino, Torino, 10124, Italy

The unmanned aerial systems (UAS) design for flight in the Martian atmosphere is thriving. This paper discusses the aerodynamic optimization of airfoils and blades at ultra-low Reynolds number conditions. In the case of airfoils, the performance predictions are carried out using unsteady Computational Fluid Dynamics (CFD). We analyzed the influence of the Reynolds number on optimal geometries and proposed a globally efficient airfoil. We computed the polar of these airfoils to generate an aerodynamic database as they are necessary for rotor reduced-order models. This work focuses on optimizing and comparing two and 3-bladed rotors. We used the Blade Element Method (BEM) to generate efficient geometries employing a genetic algorithm and evaluated the resultant geometries with higher fidelity CFD simulations. Final refinement of the presented geometries is performed with a CFD adjoint optimization.

I. Nomenclature

$C_Q = \frac{Q}{\rho \pi \Omega^2 R^5}$	=	rotor torque coefficient
$C_T = \frac{T}{\rho \pi \Omega^2 R^4}$	=	rotor thrust coefficient
$C_P = \frac{P}{\rho \pi \Omega^3 R^5}$	=	rotor power coefficient
$C_l = \frac{l}{\frac{1}{2}\rho V^2 c}$	=	airfoil lift coefficient
$C_d = \frac{d}{\frac{1}{2}\rho V^2 c}$	=	airfoil drag coefficient
c	=	airfoil chord
V	=	freestream velocity
l	=	airfoil lift
d	=	airfoil drag
Ω	=	rotation rate in radians per second
RPM	=	rotation rate in revolutions per minute
R	=	rotor radius

---

*PhD Student, Department of Mechanical and Aerospace Engineering, Politecnico di Torino, C.so Duca degli Abruzzi, 24, 10124 Torino, Italy, manuel.carreno@polito.it

†Adjunct Professor, Department of Mechanical and Aerospace Engineering, Politecnico di Torino, C.so Duca degli Abruzzi, 24, 10124 Torino, Italy, domenic.dambrosio@polito.it

Re	=	Reynolds number based on the chord
AOA	=	angle of attack
M	=	rotor tip Mach number
T	=	rotor thrust
Q	=	rotor torque
P	=	rotor power
ρ	=	air density

II. Introduction

The increasing interest in Martian exploration and the difficulties rovers face in such an irregular terrain makes Unmanned Aerial Systems (UAS) a potential alternative. Martian flight is known to be challenging for a variety of reasons. Despite Mars's gravity being about 38% of Earth's gravity, density is two orders of magnitude smaller than on Earth, which limits the capability of conventional propellers/wings to provide sufficient thrust/lift. Increasing the velocity of aerodynamic surfaces to raise aerodynamic forces, which are penalized by the low density of the atmosphere, is limited by the fact that the speed of sound on Mars is about 75% of the speed of sound on Earth at sea level. Therefore, the velocity required to achieve critical Mach numbers is lower on Mars than on Earth. In addition, high speed will also increase drag, which may require additional weight for powerful motors and lead to motor heating issues.

Several researchers have studied, numerically and experimentally, Martian Flight and, more generally, the so-called ultra-low Reynolds number regime. This range comprises Reynolds numbers ranging from 1,000 to 10,000. Kunz[1] performed extensive numerical work on efficient airfoils and rotors in these conditions. More recently, Koning[2, 3] and Bèzard[4, 5] presented detailed aerodynamic and optimization analyses of rotors in these conditions. Researchers from Japan have also pursued Martian flight publishing extensive and valuable experimental data obtained in the Martian Wind Tunnel at Tohoku University[6]. The authors have contributed to the study of this regime [7–10], where we presented the first set of numerical simulations resulting in different efficient Martian blade designs. Being a very actual topic and considering that many space agencies are aiming to achieve Martian flight, it is rare to find well-documented efficient blade geometries and the optimization procedures employed to obtain them. Therefore, this paper aims to discuss an efficient optimization strategy, stressing strengths and weaknesses and presenting the associated optimal airfoil and blade geometries. In particular, we study the different optimal geometries for two and 3-bladed rotors.

For the 2D analysis, we performed compressible Navier-Stokes simulations using an unsteady laminar solver. We have included compressibility effects because the low-temperature conditions and small gas constant of the Martian atmosphere produce a low speed of sound. Add to this the high rotational velocity required to generate thrust in a low-density environment, resulting in a subsonic but high Mach number. For these simulations, we used the commercial

Computational Fluid Dynamics (CFD) code STAR-CCM+, using its embedded Adjoint Navier-Stokes method to obtain optimal geometries for appropriate values of Mach and Reynolds numbers. We finally compared our optimized airfoils with other efficient geometries proposed in the literature [3, 4, 11] for similar operating conditions.

To design the three-dimensional blade geometry, we used two tools with different levels of fidelity. We started with the simple Blade Element Momentum Method (BEM), and we finished with a full Navier-Stokes simulation of the blades. We selected the best-performing geometries using an evolutionary algorithm (EA) to avoid local optimums, a common issue in rotor performance optimization due to the tight coupling between design and operating variables. Using low-fidelity simulation tools is necessary, as optimization with full Navier-Stokes CFD simulations is computationally expensive.

The paper also includes a three-dimensional Adjoint Navier-Stokes optimization method to enhance rotor performance. In this way, we account for aspects not considered in the BEM optimization, such as the three-dimensional flow near the tips of the blades, the variation of the operating Mach along the radial coordinate, and blade vortex interaction.

III. Airfoil optimization

In reference [8], we proceeded with an initial optimization exercise using the adjoint solver included in STAR-CCM+[12]. Using a flat plate with a thickness of 2% and rounded edges as the initial geometry, we obtained an airfoil that optimizes aerodynamic efficiency, defined as the ratio of lift to drag, for Re=3,000 and Mach=0.5. In Fig. 2, we compare the resulting airfoil shape with the clf5605 airfoil used at 0.75 of the span for the JPL's Mars Helicopter Ingenuity [2, 3], with an airfoil proposed for a Martian drone in [4] and with the NACA-6904 airfoil (6% camber at 90% chord and 4% thickness) selected in [11] as a reference for Martian conditions.

The optimized airfoil we obtained(PoliTO-1) has a very flat suction side, which concentrates the camber at the leading and trailing edges. The maximum camber is about 5.2%, very close to the trailing edge, and it shares some similarities with the NACA-6904 proposed in [11]. The average thickness is around 2%. A lower relative thickness could increase the efficiency, but we decided to stop the optimization process when the overall thickness falls below this value.

The airfoil was designed for M=0.5, Re=3000, and AOA=6º, but not necessarily for the rest of the polar and other conditions. However, comparing its performance with those declared by other authors for an optimized airfoil for similar conditions [4], the result appeared to be promising, as shown in Fig. 1. It is clear how the adjoint optimized airfoil achieves the best improvement for Reynolds numbers close to 3000, while for Re = 10000, its performance starts to degrade, possibly due to its aggressive shape.

In Refs.[9, 10], we further refine this airfoil. We interpolated the airfoil PoliTO-1 using a high-order polynomial fitting and repeated the adjoint-based optimization, this time for a Reynolds number of 10,000 and an angle of attack of 4 degrees. Details on the optimization algorithm can be found in Ref. [10]. The resulting airfoil, PoliTO-2, shows a slightly
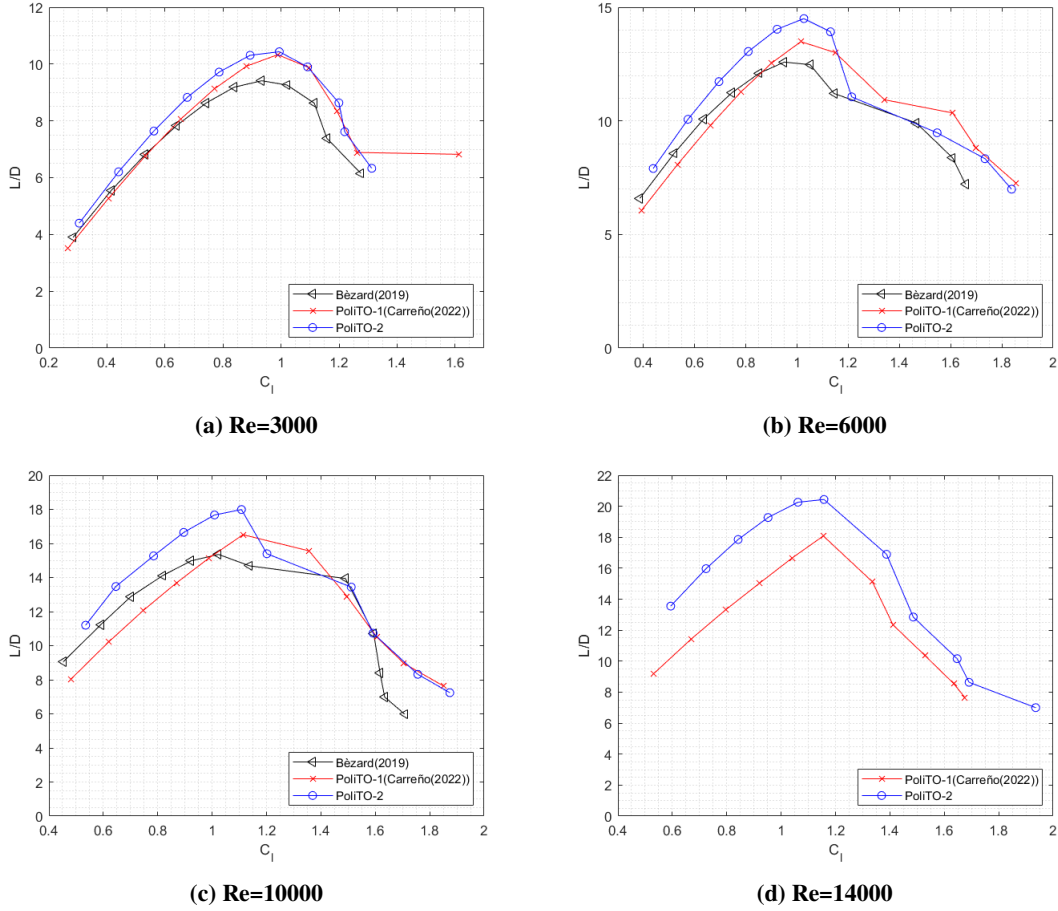
(a) Re=3000

(b) Re=6000

(c) Re=10000

(d) Re=14000

Fig. 1 Comparison of aerodynamic efficiency at different Reynolds numbers: PoliTO1[8] vs Bèzard(2019)[4] vs PoliTO-2.

less flat suction side with curvature more evenly distributed than PoliTO-1, as shown in Fig. 2. The maximum camber position is farther from the trailing edge, and the average thickness is around 2%. In this case, we can appreciate how the airfoil outperforms the airfoil presented by [4] in all operating conditions. Regarding the improvements, compared with PoliTO-1, we notice a significant enhancement in the attached regime for all Reynolds numbers. Considering that efficient rotors rarely present Cl coefficients much larger than 1, as shown in [4], it is expected that this airfoil will produce a significant increase in the efficiency of the blades.

IV. Blade optimization

We performed an initial optimization using an in-house BEM solver implemented in MATLAB (see Ref. [13] and Refs. 14 and 15 for details about its development and validation). We also included a classical angular momentum viscous swirl correction as its effects might be significant in the ultra-low Reynolds number regime as suggested in [1].

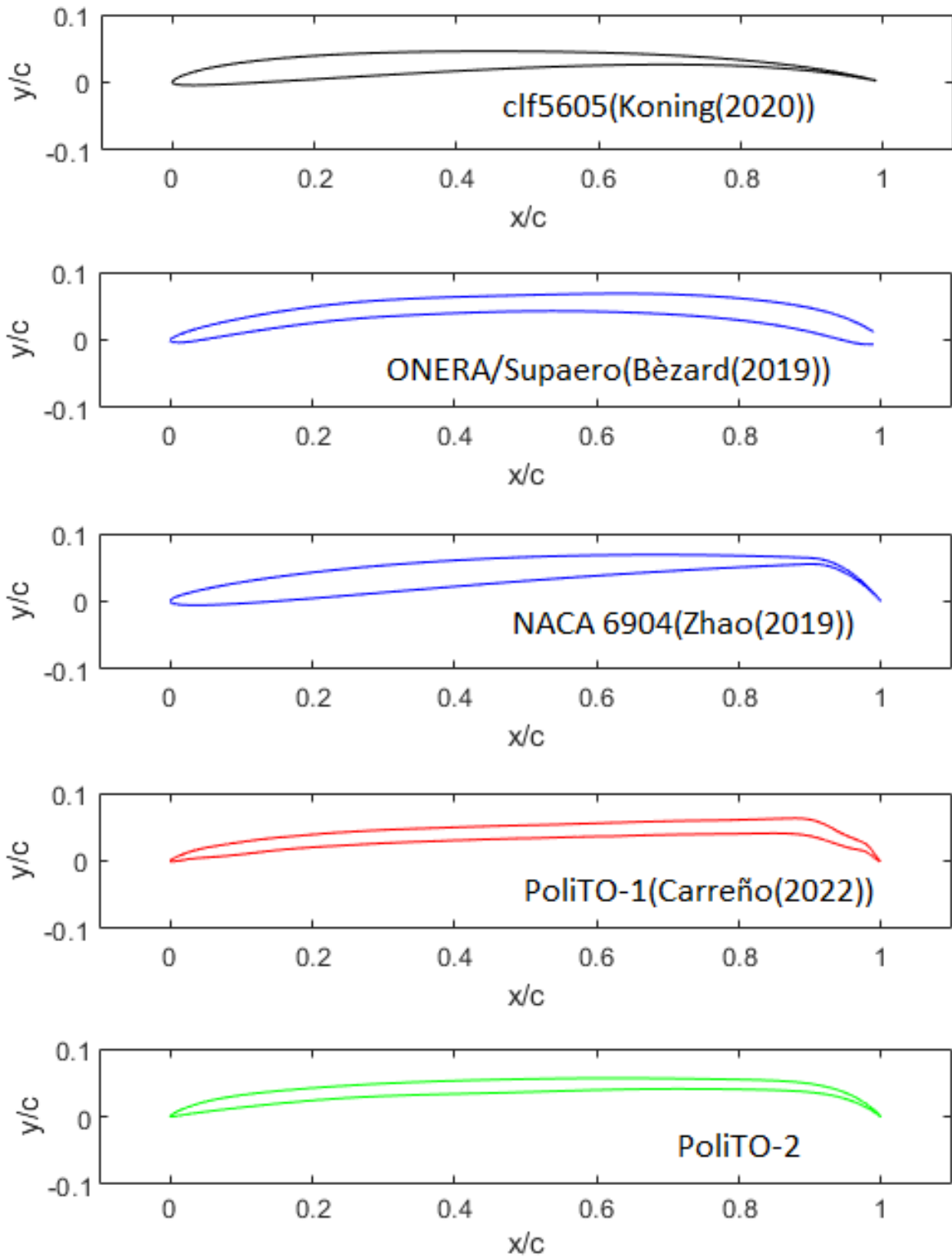We computed the polar of PoliTO-2 airfoil for Reynolds numbers 3,000 to 14,000 for angles of attack between 0

Fig. 2   Different airfoil geometries reported in literature.

and 10 degrees. The polar was computed for a Mach number of 0.5. This value of the Mach number is the expected value near 75% of the radius where more significant values of thrust and torque are expected. Bèzard [4] reports minimal variations of the aerodynamic efficiency for tip Mach numbers below 0.7. Therefore, we used Prandtl-Glauert's correction to adjust the lift and drag values.

We parametrized both chord and twist distributions using 4 degrees of freedom and spline interpolation along the radial coordinate. The rotor diameter is fixed at 0.4 m, while the rotation rate is considered a design parameter.

Initially, we adopted an Evolutionary Algorithm (EA) to avoid local optima. We then optimized each geometry using a gradient-based approach to find distinct local optima. The objective function was defined as the power loading employing the partial weight penalization suggested in [9] as shown in equation 1:

$$L = \frac{T - \sigma W_{Mars}}{P} \tag{1}$$

Using the net thrust ($\sigma = 1$) prevents the rotor from having too large solidities that would be counterproductive because of their weight. However, Ref.[8] shows how this correction results in large aspect ratios and very thin blades, which could compromise structurally the blade. In this work, we select $\sigma = 0.5$ to to trade-off both effects. The objective function includes a penalization function that prevents the thrust value from going below 1.1 N. This thrust value will allow lifting a mass of 300 g on Mars; therefore, the mass budget for the complete quadcopter would rise to 1.2 kg. We repeated the algorithm for 2-bladed and 3-bladed rotors. Figure 5 shows the resultant geometries.

Table 1   Optimal BEM geometries.

Blade-Solver	Omega(rpm)	Thrust(N)	Torque(Nm)	T/P (N/W)
2 Blades-BEM	6596	1.10	0.0414	0.0385
2 Blades-CFD	6596	1.073	0.0433	0.0359
2 Blades-CFD	6678	1.10	0.0444	0.0354
3 Blades-BEM	6518	1.10	0.0432	0.0373
3 Blades-CFD	6518	1.057	0.0440	0.0352
3 Blades-CFD	6649	1.10	0.0458	0.0345

We performed Navier-Stokes simulations of the blades with a twofold aim. First, to verify the capability of the BEM code to predict the twist distribution, and second to understand the influence of different geometries in the three-dimensional aerodynamics around the rotating blades. All CFD simulations adopt a laminar model, though a separation-induced transition may be present on the blade sections at the highest Reynolds number. The maximum Reynolds number for their specified rotational speed is 14,000 at a radial position of 16 cm for the 2-bladed rotor and 10,000 for the 3-bladed rotor. However, simulations reveal that the flow remains attached; therefore, the hypothesis that transition will only occur on the wake at these Reynolds numbers seems reasonable. We will work under the assumption
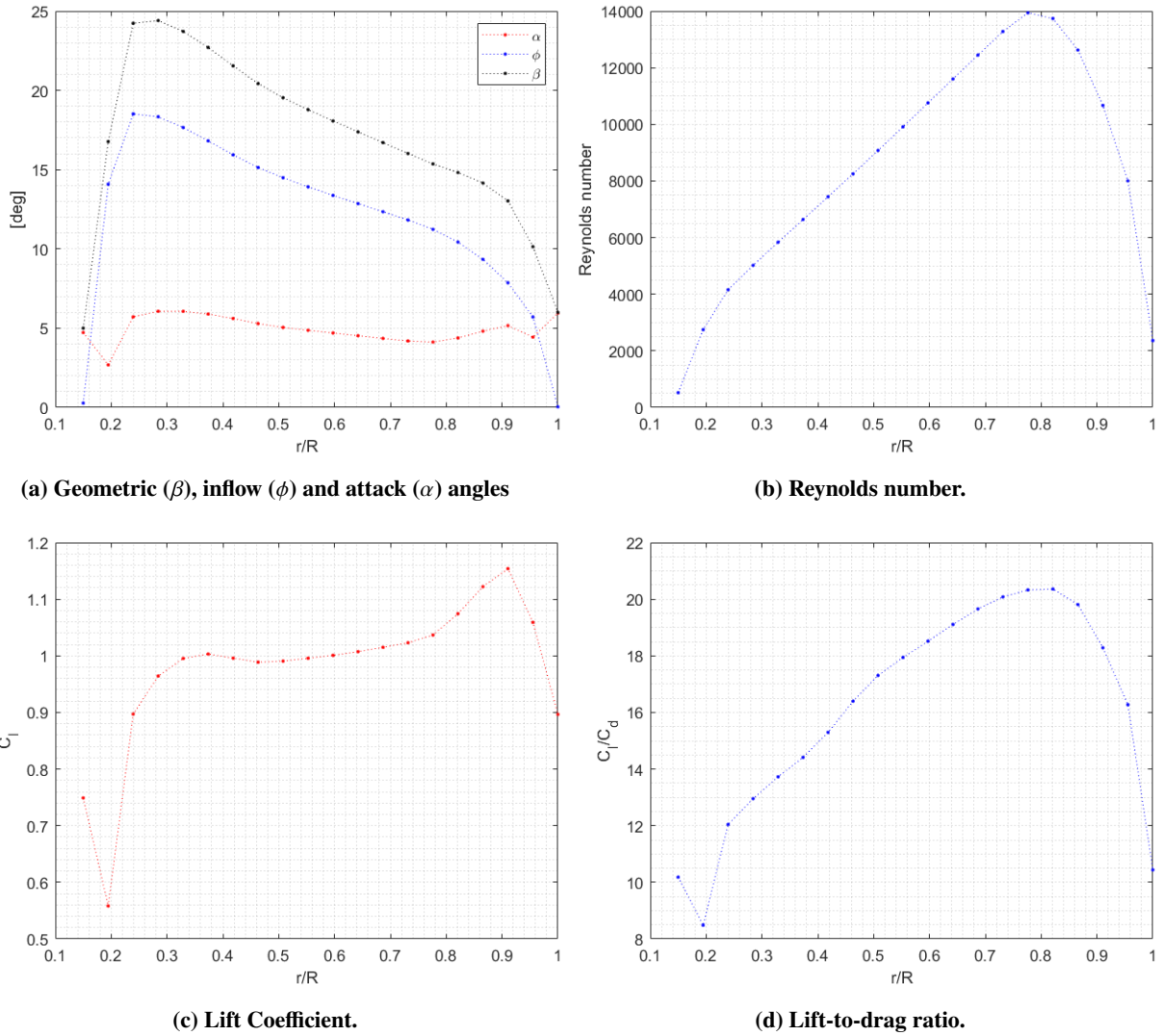
(a) Geometric (β), inflow (φ) and attack (α) angles

(b) Reynolds number.

(c) Lift Coefficient.

(d) Lift-to-drag ratio.

Fig. 3   BEM: local results on the 2-bladed optimal geometry.

that Navier-Stokes equations are a reliable mathematical model to predict rotors' performance in the Mars atmosphere, as shown in [4].

We validated the laminar solver of STARCCM+ in [7] by comparing CFD simulations with experimental results presented in [6]. The latter refers to an experimental campaign at the Martian Wind Tunnel (MWT) of Tohoku University on a triangular wing invested by a current at ultra-low Reynolds numbers. The grids for the rotor simulations presented in this paper contain approximately 12 million cells. We used a sliding grid approach with a second-order implicit time-dependent scheme and a time step equivalent to a blade rotation of 2.5 degrees per temporal iteration for the first ten revolutions and a time step corresponding to 0.5 degrees per temporal iteration for the last four revolutions. Fourteen rotor revolutions are sufficient for thrust and torque convergence, as shown in [4, 10]. The atmospheric conditions for our simulations are the average Mars atmospheric conditions reported in Bézard [5], corresponding to a temperature of
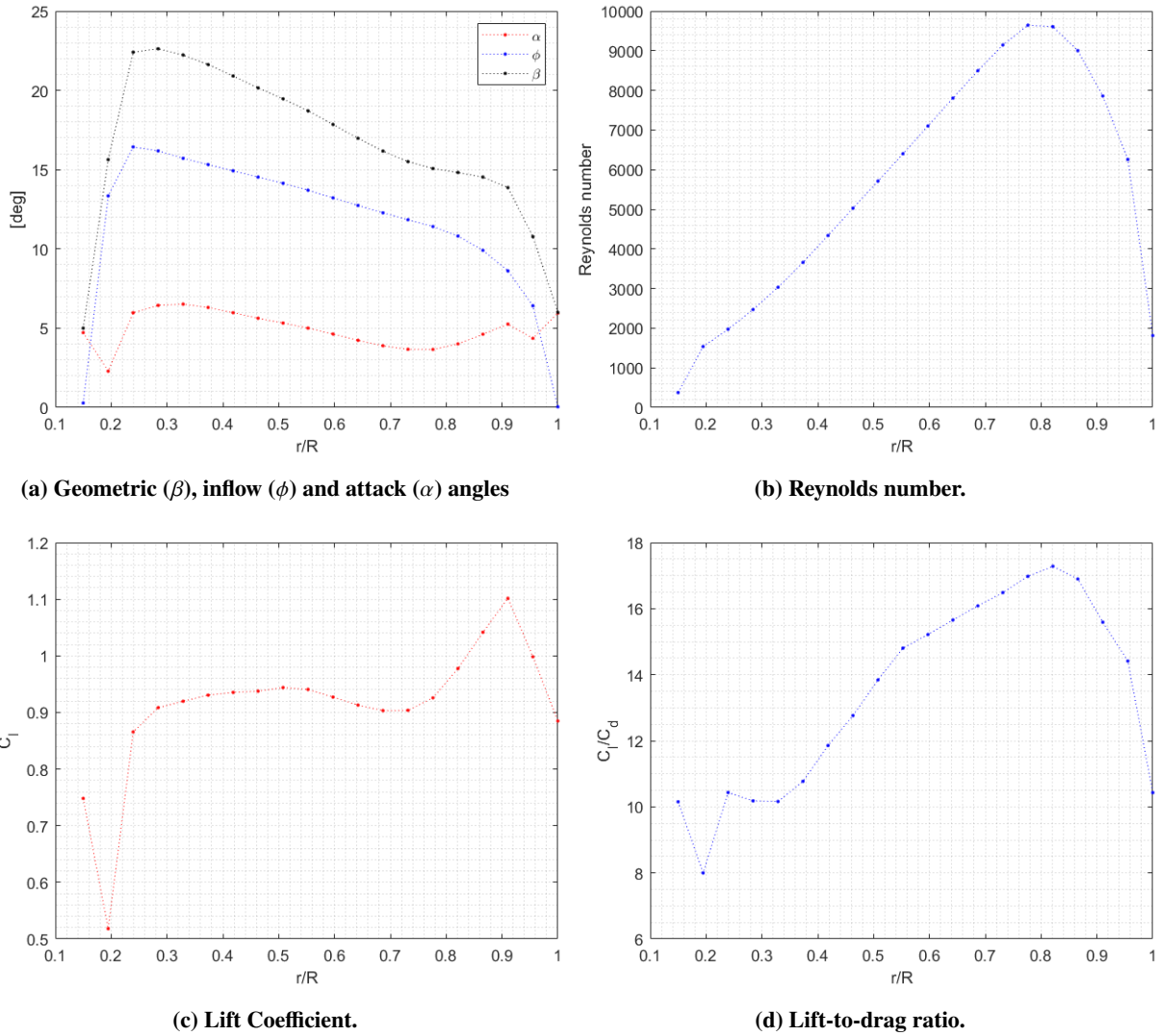
(a) Geometric (β), inflow (ϕ) and attack (α) angles

(b) Reynolds number.

(c) Lift Coefficient.

(d) Lift-to-drag ratio.

Fig. 4   BEM: local results on the 3-bladed optimal geometry.

-63ºC and a pressure of 660 Pa. The atmosphere is idealized as pure carbon dioxide.

Fig. 6 shows the Q-criterion for the two and 3-bladed rotors. We can appreciate how the boundary layer on the blade remains attached until the trailing edge, where a vortex-shedding regime starts. In the case of the 3-bladed rotor, we can appreciate how the tip vortex passes much closer to the surface of the following blade. Therefore, the estimated angles of attack predicted by the BEM theory may not accurately estimate those revealed by the CFD simulations. This fact could deviate the BEM optimal design from the actual optimal design.

Table 1 shows the performance predictions performed by the CFD and BEM solvers. The CFD thrust values slightly under-predict the BEM values and over-predicting torque values. However, the differences are relatively small, around 5% for the thrust and 3% for the torque. It is also interesting to note that the power loading for the 2-bladed rotor is slightly higher than the 3-bladed rotor, both in CFD and BEM predictions. In any case, the difference between both
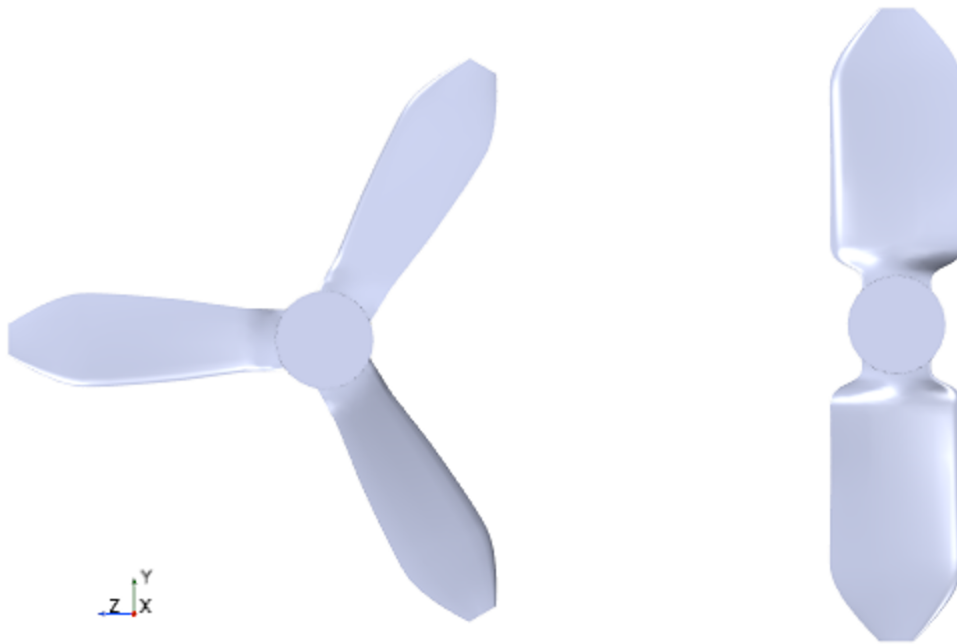
Fig. 5   BEM optimal geometries.

CFD simulations is less than 3%, and there are some mechanical advantages of using 3-bladed rotors, such as avoiding specific vibration axis as stated in [4].
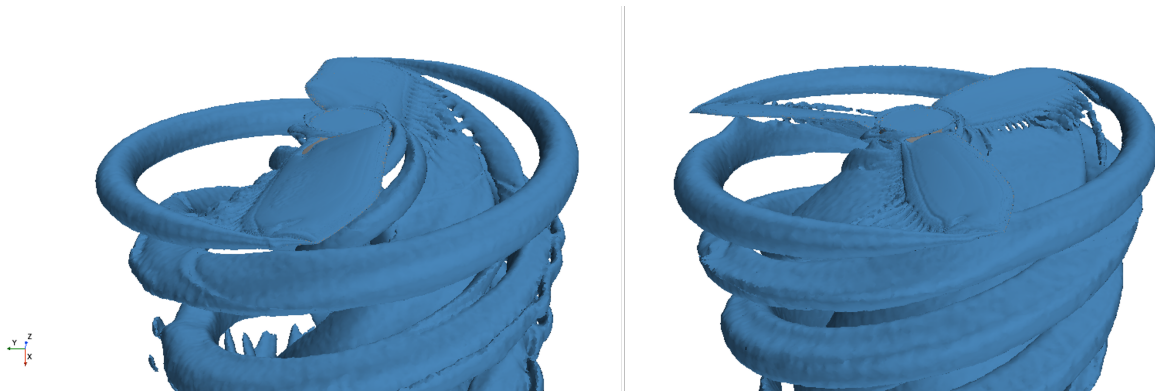

Fig. 6   Q-criterion iso-surface obtained with unsteady solver for 2-blade rotor (left) and 3-blade rotor (right).

V. Adjoint-based Optimization

The steady adjoint solver embedded in the commercial CFD package STAR-CCM+ [12] is used to calculate the sensitivity of an objective function to the design parameters d_i. The objective function is defined as follows:

$$X = \frac{T^{3/2}}{Q} \qquad (2)$$

This function allows the use of simulations with constant rotation rates, ensuring that even if the blade thrust decreases, the rotation rate can be increased, still improving the energy consumption of the blades. That noticeably accelerates the convergence of the Navier-Stokes equations solutions without the need to adjust the rotation rate at each iteration.

We defined the Control points, shown in Fig. 8 with an offset of 5 mm from the blade surface. Their displacement along the direction of the gradient vector following a so-called steepest descent approach increases the objective function. We preferred to avoid using the blade as a response surface because such a choice may create dimples while moving the offset points generates smoother wall surfaces. Of course, we apply a floating condition at the blade boundary. Control points are free to move in the tangential and axial directions but not in the radial direction to avoid rotors with larger diameters. In this way, airfoil geometry, twist distribution, and chord distribution are allowed to change until reaching maximum efficiency or minimum airfoil thickness. Equation (3) shows the rule governing the displacement of the control points in each adjoint iteration:

$$d_i = d_{i-1} + \frac{h_{step}\nabla X}{max(|\nabla X|)} \qquad (3)$$

Table 2   Comparison between BEM and CFD-Adjoint optimal geometries.

Geometry-Solver	Omega(rpm)	Thrust(N)	Torque(Nm)	P (W)
2B-BEM-CFD	6678	1.10	0.0444	31.07
2B-Adjoint-CFD	7042	1.10	0.0403	29.72
2B-Difference(%)	5.5	0	-9.2	-4.4
3B-BEM-CFD	6649	1.10	0.0458	31.89
3B-Adjoint-CFD	6504	1.10	0.0433	29.91
3B-Difference(%)	-2.2	0	-5.5	-6.2

The unsteady simulation shown in the previous section reveals that the flow on the blade is attached and stable in a reference frame that rotates with it. The only source of instability is a vortex spreading downstream of the trailing edge. Therefore, the Navier-Stokes (primal) simulation adopts the Moving Frame of Reference (MFRA) approach described in [16], where the Navier-Stokes equations frame of reference rotates with the blade. Despite the steady-state nature of the technique and the imperfect resolution of the flowfield at the trailing edge, it is possible to reproduce the boundary layers and first tip vortex revolutions with acceptable accuracy. The general consistency between steady-state and unsteady solutions suggests that an optimal shape obtained through the steady-state approach will also improve performance in time-accurate simulations. As shown in [16], the computational cost of the MFRA approach is about

an order of magnitude lower than the unsteady sliding-grid approach. That is due to the use of a periodic boundary condition, which allows the simulation of only one blade, thus dividing the number of cells by two in the case of a two-bladed simulation and by three in the three-bladed simulations. Also, since we keep the adjoint step at 0.5 mm, the convergent solution of one adjoint iteration is a good initial condition for the next adjoint iteration.

These steady-state calculations adopt a simplified domain that takes advantage of the periodic symmetry of the problem. The outer static region has the shape of a half-trunk of a cone. The solution of the Navier-Stokes equations in the rotating reference frame takes place in an inner cylindrical domain to model the rotation of the blade. In this second computational domain, the formulation of the governing equations of fluid dynamics contains the centrifugal and Coriolis accelerations as source terms, as explained in [17]. To increase the convergence rate, we insert a free stream in the axial direction with a velocity of 0.1 m/s, as shown in [16] for a small-scale rotor. Figure 7 shows the boundary conditions and periodic interfaces that define the problem.

The grid used for these simulations is equivalent to the medium grid shown in the previous section in the region near the blades. The wake region is slightly less refined to promote convergence by damping the instability observed downstream of the trailing edge. The number of cells for these simulations is around 6 million cells.
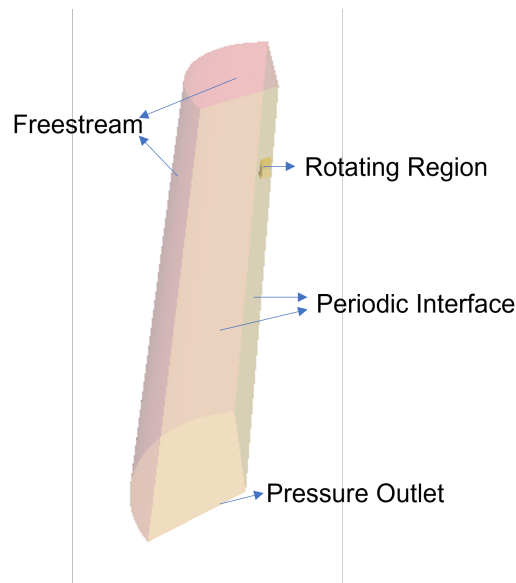

Fig. 7 Boundary conditions and computational setup for MFRA for the three-bladed rotor.

Figure 8 shows the lattice of points that the morpher uses to deform the grid. After the optimization process, adjoint sensitivities to the objective function suggest reducing the curvature at the trailing edge and the angle of attack in the 75%-90% radial coordinate region. Figure 9 displays the final shape of the blade after 16 adjoint iterations. Figs. 10 and 11 show the airfoil geometry at different radial stations for both blades. We notice that towards the tip, where the Reynolds number is the largest, the airfoil geometry has a reduced camber and is evenly distributed throughout the chord. It is also noticeable how the maximum camber position moves towards the leading edge as the Reynolds number

increases. The angle of attack got smaller along most of the blade span except in the vicinity of the tip region. It is interesting to see how the modifications introduced by the adjoint solver move in the same direction for both blades, even for very different planforms and rotation rates.

To compare the performance of the final blade geometry with others, we performed a full unsteady Navier-Stokes simulation with the same grid settings that we used to evaluate the optimal BEM geometry. Table 2 shows that the adjoint method further improves the two and three-bladed rotor performance. In the case of the two-bladed rotor, we can appreciate a reduction in power consumption of 4.4% in comparison with the BEM optimal blade. Interestingly, the new geometry tends towards a lower torque configuration operating at a higher rotational speed. However, due to the choice of the objective function, the result is a decrease in energy consumption. Similarly, the three-bladed design has a slightly more significant improvement in power consumption than the BEM baseline design achieving a 6.2% reduction. In this case, the optimization converts the geometry into a slightly lower torque configuration with a slight decrease in rotation rate, further improving the blade's efficiency.

Both rotors present a figure of merit around 0.60. Such a result is consistent with the experimental and numerical values that Koning [18] found for the Martian Helicopter rotor for an equivalent blade loading of 0.11. Considering that our radius is limited to 0.2 m compared with the 0.605 m of the Martian rotor blade, the results look promising as increasing the rotor diameter could potentially improve the performance due to the increase in the Reynolds number, reducing the rotation rate and chord distribution for a constant tip velocity. The blade geometry proposed by Bézard [5] for the upper rotor of the 300 g coaxial helicopter configuration has a figure of merit of 0.55, 10% lower compared to our rotors. However, they limit the radius to 0.15 m, and thus the results may not be comparable. In any case, we can conclude that the proposed blade design procedure generates rotor geometries that are at least as performing as those designed using other techniques based on vortex methods.
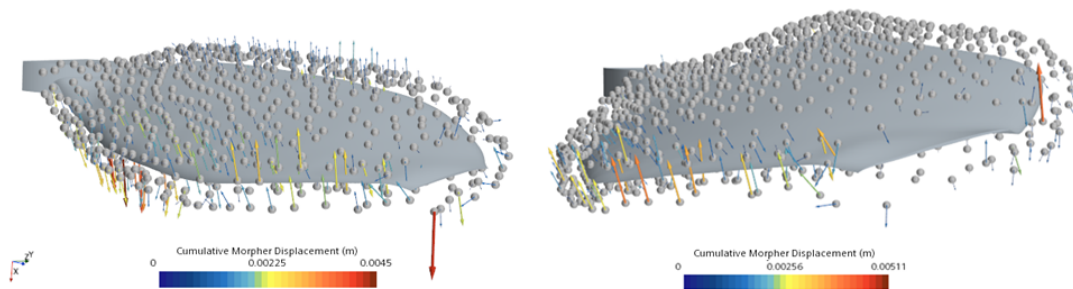

Fig. 8   Morpher control point displacements after the adjoint optimization process for the two-bladed rotor (left) and three-bladed rotor (right).
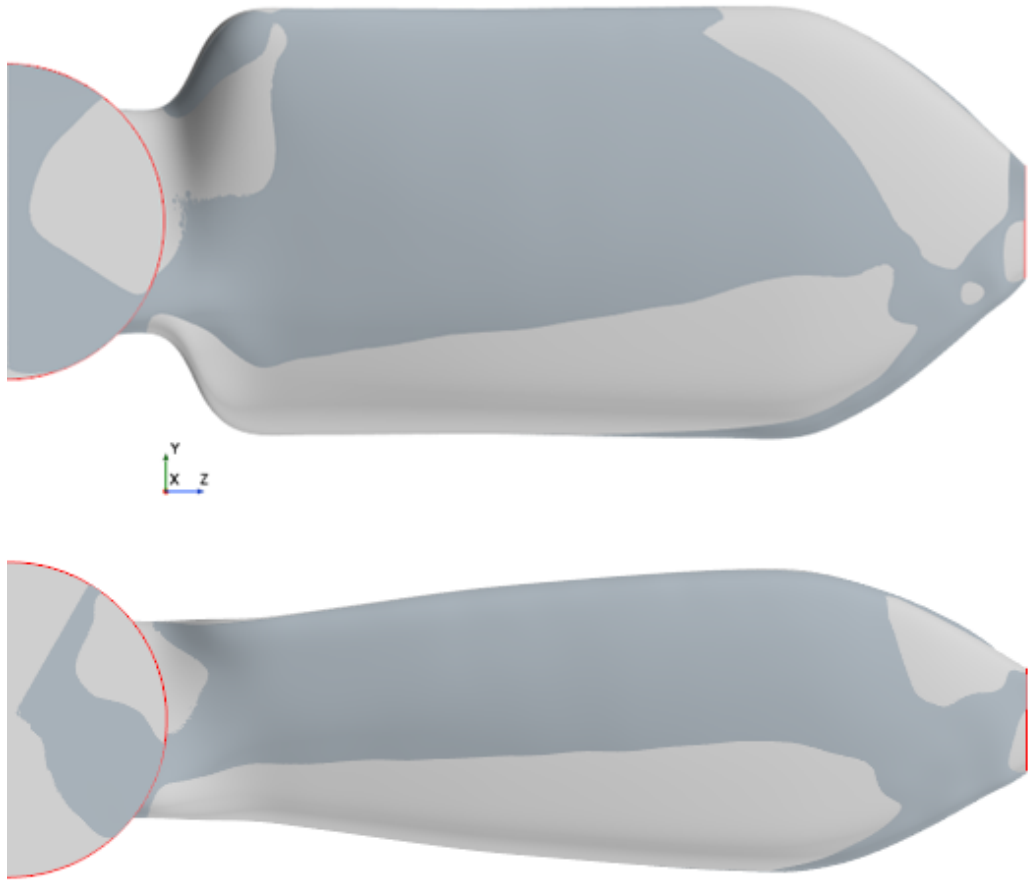
Fig. 9   Comparison between the original (light grey) and final morphed surface (dark grey) for the two-bladed rotor (left) and three-bladed rotor (right).

r=0.05m

r=0.09m

r=0.13m

r=0.17m

Fig. 10   Normalized airfoil sections at different radial stations after adjoint optimization. Two-bladed rotor.

r=0.05m

r=0.09m

r=0.13m

r=0.17m

Fig. 11   Normalized airfoil sections at different radial stations after adjoint optimization. Three-bladed rotor.

VI. Conclusions

The multi-fidelity optimization procedure described in this paper provides aerodynamically efficient rotors for a different number of blades and chord distributions. The improvement in the efficiency of the airfoil reflects positively on the efficiency of the final blades compared to previous designs. The hovering performance of two and three-bladed rotors have subtle differences, below 1%. This finding shows how the three-bladed rotors could be a competitive solution that avoids the problem of presenting a specific vibration axis.

Another interesting conclusion is how the implemented BEM solver allows relatively accurate blade evaluations and how this accuracy is reduced in the case of three-bladed simulations, possibly due to the increased blade vortex interaction. We can also appreciate how in the case of the 3-bladed rotor, the adjoint solver provides a more significant improvement than the 2-bladed simulations. This is probably also related to the inability of the BEM solver to capture blade vortex interaction and the enhanced importance of the tip correction.

Future work includes the structural analysis of these blades to impose more realistic restrictions on the design. This methodology provides good-performing blades for very different geometries, suggesting that the planform of the blade only mildly affects the efficiency as long as an appropriate twist and airfoil distribution are chosen.

References

[1] Kunz, P. J., "Aerodynamics and design for ultra-low Reynolds number flight," Ph.D. thesis, Standford University, 2003.

[2] Koning, W. J., Johnson, W., and Allan, B. G., "Generation of Mars Helicopter Rotor Model for Comprehensive Analyses," *AHS Aeromechanics Design for Transformative Vertical Flight*, 2018.

[3] Koning, W. J., Romander, E. A., and Johnson, W., "Optimization of Low Reynolds Number Airfoils for Martian Rotor Applications Using an Evolutionary Algorithm," *AIAA Scitech 2020 Forum*, 2020, p. 0084.

[4] Bézard, H., Desert, T., Moschetta, J.-M., and Jardin, T., "Aerodynamic design of a Martian micro air vehicle," *EUCASS 2019*, MADRID, Spain, 2019. URL https://hal.archives-ouvertes.fr/hal-02397054.

[5] Bézard, H., Désert, T., Jardin, T., and Moschetta, J.-M., "Numerical And Experimental Aerodynamic Investigation Of A Micro-UAV For Flying On Mars," *76th Annual Forum & Technology Display*, 2020.

[6] Munday, P. M., Taira, K., Suwa, T., Numata, D., and Asai, K., "Nonlinear lift on a triangular airfoil in low-Reynolds-number compressible flow," *Journal of Aircraft*, Vol. 52, No. 3, 2015, pp. 924–931.

[7] Carreño Ruiz, M., and D'Ambrosio, D., "Validation and application of aerodynamic simulations in the Martian atmosphere," *26th Conference of the Italian Association of Aeronautics and Astronautics-AIDAA 2021*, 2021.

[8] Carreño Ruiz, M., and D'Ambrosio, D., "Aerodynamic Optimization of Quadrotor Blades Operating in the Martian Atmosphere," *AIAA SCITECH 2022 Forum*, 2022. https://doi.org/10.2514/6.2022-0743.

[9] Carreño Ruiz, M., Bellelli, F., and D'Ambrosio, D., "Numerical Investigation on the Aerodynamic Design of Quadrotor Blades Operating in the Martian Atmosphere," *EUCASS 2022*, 2022. https://doi.org/10.13009/EUCASS2022-4637.

[10] Carreño Ruiz, M., and D'Ambrosio, D., "Aerodynamic Optimization and Analysis of Quadrotor Blades Operating in the Martian Atmosphere," *Aerospace Science and Technology*, 2022. https://doi.org/10.1016/j.ast.2022.108047.

[11] Zhao, P., Quan, Q., Chen, S., Tang, D., and Deng, Z., "Experimental investigation on hover performance of a single-rotor system for Mars helicopter," *Aerospace Science and Technology*, Vol. 86, 2019, pp. 582–591.

[12] Siemens Digital Industries Software, "Simcenter STAR-CCM+ User Guide v. 2019.3," , Siemens 2019.

[13] Scanavino, M., "Design and testing methodologies for UAVs under extreme environmental conditions," Ph.D. thesis, Politecnico di Torino, 2021.

[14] Carreño Ruiz, M., Manavella, A., and D'Ambrosio, D., "Numerical and experimental validation and comparison of reduced order models for small scale rotor hovering performance prediction," *AIAA SCITECH 2022 Forum*, 2022. https://doi.org/10.2514/6.2022-0154.

[15] Manavella, A., "Low Reynolds number propeller performance validation by CFD analysis and reduced order models," Master's thesis, Politecnico di Torino, 2021.

[16] Carreño Ruiz, M., Scanavino, M., D'Ambrosio, D., Guglieri, G., and Vilardi, A., "Experimental and numerical analysis of hovering multicopter performance in low-Reynolds number conditions," *Aerospace Science and Technology*, Vol. 128, 2022, p. 107777. https://doi.org/10.1016/j.ast.2022.107777.

[17] Carreño Ruiz, M., "CFD simulation of propellers: Best Practices Analysis," Master's thesis, Politecnico di Torino, 2019.

[18] Koning, W. J., Johnson, W., and Grip, H. F., "Improved Mars helicopter aerodynamic rotor model for comprehensive analyses," *AIAA Journal*, Vol. 57, No. 9, 2019, pp. 3969–3979.